AGU PUBLICATIONS

Geophysical Research Letters

RESEARCH LETTER
10.1002/2017GL075430

Key Points:
- Realistic bathymetry alters the vertical structure of ocean eddies
- Knowing the correct structure facilitates projecting surface fields downward in the water column
- The results explain a number of diverse observations, from current meters, satellite measurements, and models

Supporting Information:
- Supporting Information S1

Correspondence to:
J. H. LaCasce,
j.h.lacasce@geo.uio.no

Citation:
LaCasce, J. H. (2017). The prevalence of oceanic surface modes. *Geophysical Research Letters*, *44*, 11,097–11,105. https://doi.org/10.1002/2017GL075430

Received 24 AUG 2017
Accepted 13 OCT 2017
Accepted article online 18 OCT 2017
Published online 11 NOV 2017

The Prevalence of Oceanic Surface Modes

J. H. LaCasce[1]

[1]Department of Geosciences, University of Oslo, Oslo, Norway

Abstract Satellite observations have revolutionized oceanography, capturing diverse phenomena over much of the globe. However, it remains to understand how surface fields, like sea surface height, reflect the motion occurring at depth. The vertical structure of ocean eddies is often expressed in terms of "baroclinic modes," which are basis functions derived assuming a flat ocean bottom. Bathymetry alters the modes though, weakening the bottom velocities. Using analytical solutions, we demonstrate that with realistic bathymetry and/or bottom friction, the bottom velocities are nearly zero. The resulting "surface modes" should be ubiquitous in the ocean. This would explain the dominant mode of variability obtained from globally distributed current meter data and is consistent with energy spectra derived from sea surface height data. The results yield a simple way to infer subsurface velocities from satellite data and suggest that ocean analyses should be made in terms of surface modes and topographic waves.

Plain Language Summary Observations of the sea surface from satellites have revolutionized oceanography. But it is important to understand how the surface fields, such as sea height and surface temperature, reflect the motion occurring at depth. Traditionally, oceanographers have represented the vertical structure of ocean currents using "modes." One of these, for example, does not vary with depth. The present work demonstrates how these modes change when realistic bottom topography is taken into account. The results suggest a simple way to predict subsurface velocities and have implications for our understanding of ocean dynamics.

1. Introduction

Time-dependent features in the ocean are generally referred to as "eddies." At low latitudes, ocean eddies are often wave-like and trapped near the equator, with scales of thousands of kilometers. The eddies are smaller at middle and high latitudes, having scales comparable to the "Rossby deformation radius," typically from 10 to 100 km. Extratropical eddies also tend to be more nonlinear than at low latitudes, having advective (rotational) speeds in excess of their propagation speeds (Chelton et al., 2011). Nevertheless, the propagation speeds at midlatitudes are comparable to those of linear planetary (Rossby) waves, and as such, Rossby wave theory is relevant for understanding their dynamics.

Much of what we know about ocean eddies comes from satellite data, particularly from altimetric measurements of dynamic sea surface height (SSH) (e.g., Wunsch, 2015). Gridded global surveys of SSH are now available with 1/4° resolution (the spatial smoothing applied to SSH data reduces its actual resolution, to roughly 100 km). But it remains to fully understand how SSH reflects the motion occurring at depth.

In a seminal paper, Wunsch (1997) employed data from globally distributed current meters to determine the vertical structure of subinertial currents, projecting the subsurface velocities onto "baroclinic modes." These are orthogonal basis functions, derived using climatological density and assuming a flat bottom. The gravest modes are the "barotropic" (BT), with depth-invariant velocities, and the "first baroclinic" (BC1), whose velocities change sign once in the vertical. Wunsch found that in many locations, over 80% of the subsurface variance was captured with the BT and BC1 modes alone. This was in line with earlier theoretical work, which suggested that nonlinear interactions cause energy to accumulate in these modes (Fu & Flierl, 1980). BC1 has a larger amplitude at the surface, so Wunsch concluded that SSH anomalies probably reflect that mode. Consistently, SSH anomalies have lateral scales proportional to the Rossby deformation radius (Stammer, 1997), the scale associated with BC1.

Interestingly, Wunsch also found that the primary empirical orthogonal function (EOF1), calculated with the same current meter data, often did not resemble either the BT or BC1 modes. Rather, it decayed monotonically

with depth, without changing sign. He suggested that this could be due to having a combination of BT and BC1 modes present, in roughly equal proportion.

The vertical EOFs were reexamined by de La Lama et al. (2016), using a larger current meter data set. EOF1 exhibited the same vertical structure, decaying monotonically with depth to a value near zero at the bottom. The primary EOF was found to capture a substantial fraction of the subsurface variance, typically over 80% in many locations. But while the structure differed from BC1, it was very similar to another type of mode, which we refer to as a "surface mode."

Surface modes are baroclinic modes that are obtained over steep or rough bathymetry. Having bottom relief alters the bottom boundary condition for the baroclinic mode calculation, because the horizontal and vertical velocities are coupled when the lower surface is not flat. This has several consequences. For one, the depth-varying modes become more surface intensified and have weaker horizontal flow at the bottom, to minimize cross-isobath motion (Charney & Flierl, 1981; Rhines, 1970; Samelson, 1992; Veronis, 1981). The surface modes are obtained in the limit of very steep bathymetry, having zero horizontal flow at the bottom. Bathymetry also affects the BT mode, which is replaced by bottom intensified topographic waves. Surface modes might be expected near the continental margins, where topographic waves are observed (Garrett, 1978; Pickart, 1995), or over mid-ocean ridges (Fu et al., 1982). The flat bottom baroclinic modes, on the other hand, ought to apply in the ocean interior, over the abyssal plains. But EOF1 resembles the gravest surface mode in most extratropical regions, regardless of bathymetry (de La Lama et al., 2016).

As seen hereafter, the explanation concerns what constitutes "steep" bathymetry. With even modest bottom slopes, the modal structure shifts from flat bottom to surface modes. Bottom friction has a similar effect, reducing the bottom flow. As such, surface modes should be preferred to traditional baroclinic modes nearly everywhere in the ocean.

2. Results

2.1. Vertical Modes Over Bathymetry

Oceanic motion at scales of tens to hundreds of kilometers is governed approximately by the "quasi-geostrophic potential vorticity" (QGPV) equation (Charney & Flierl, 1981; Pedlosky, 1987). Rossby waves are a time-dependent solution of the linear QGPV equation. The latter is separable, allowing the definition of an equation which determines the vertical structure. With appropriate surface and bottom boundary conditions, this constitutes a Sturm-Liouville problem, yielding a complete set of orthogonal eigenvectors—the baroclinic modes (Gill, 1982). The modes are often obtained numerically, using climatological density (Kundu et al., 1975; Wunsch, 1997). The usual assumption is that the bounding upper and lower surfaces are flat, preventing vertical motion.

The modal problem can also be solved analytically with certain idealized density profiles. One is a constant stratification, corresponding to a density which increases linearly with depth. As is well known, the eigenvectors over a flat bottom are cosine functions (Gill, 1982; Pedlosky, 1987). That the solutions change if the bottom is sloping was first shown by Rhines (1970). We will reexamine his solution, to test the dependence on the bottom slope. As in that work, we assume that the lower boundary is a smooth incline, sloping in the north-south direction. The slope direction does not affect the results for most wave vectors. Only when the wave vector is parallel to the topographic gradient, so that the bottom velocities are parallel to the isobaths, does the slope's influence vanish. The details are given in section S1 of the supporting information.

The first eigenvectors for a 100 km wave with different bottom slopes are shown in Figure 1a. The stratification is set so that the inverse of the first eigenvalue, the mode's deformation radius, is approximately 40 km, a typical value at midlatitudes. With a bottom slope of 10^{-6}, the mode is essentially like that with a flat bottom: a half cosine wave with equal amplitudes at the surface and bottom. But the bottom amplitude decreases as the slope is increased, and with a slope of 10^{-3} the amplitude is near zero. This is the gravest surface mode with constant stratification. The change in the modal structure is as expected, but it is notable that the surface mode obtains with a fairly modest slope.

The problem can also be solved analytically with exponential stratification, which is a more realistic representation for oceanic density (Munk, 1966; Wunsch, 2015). We derive this solution, assuming a stratification with a surface value of 10^{-2} s^{-1} and an *e*-folding depth of 1,000 m, in the supporting information.

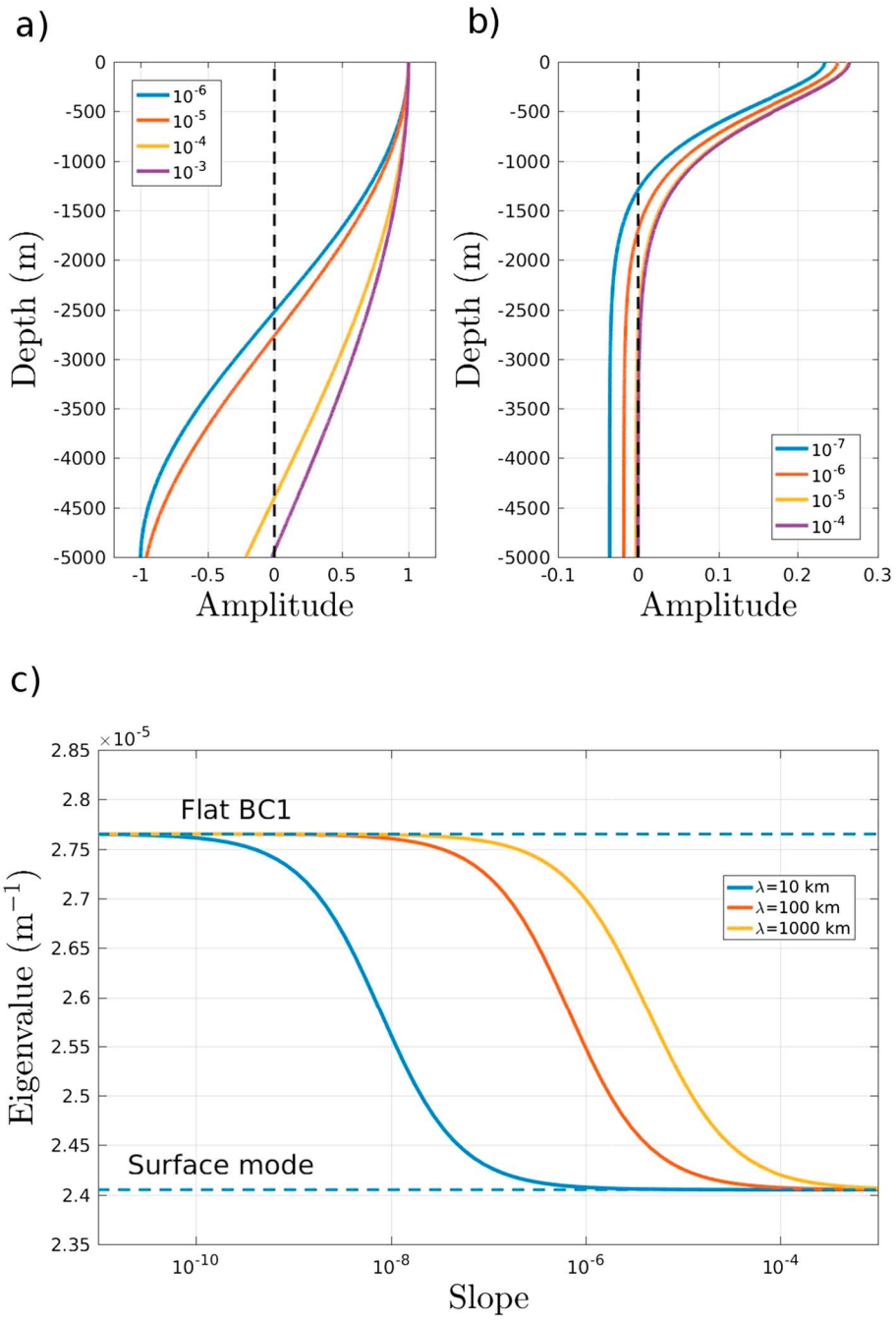

Figure 1. The first baroclinic eigenvectors with (a) constant stratification and (b) exponential stratification, for a 100 km wave over different bottom slopes. (c) The first baroclinic eigenvalue as a function of bottom slope with exponential stratification, for different wavelengths. The eigenvalues for the flat bottom BC1 and the gravest surface mode are shown for comparison.

The first eigenvectors for a 100 km wave are shown in Figure 1b. These are surface intensified, decaying rapidly over the upper 1,000 m. With a slope of 10^{-7}, the eigenvector has a zero crossing near 1,300 m and opposed flow at the bottom, as over a flat bottom (Garrett & Munk, 1972; LaCasce, 2012; Zang & Wunsch, 2001). But with a slope of 10^{-5}, the bottom flow is near zero (the result with a slope of 10^{-4} is nearly the same). Thus, the bottom velocity vanishes with a weaker slope with exponential solution than with constant stratification.

The greater sensitivity to bottom slope with exponential stratification can be understood as follows. The bottom boundary condition is determined by the quasi-geostrophic (QG) density equation (Pedlosky, 1987; equation (3) in section S1 of the supporting information). From this, one can see that the vertical

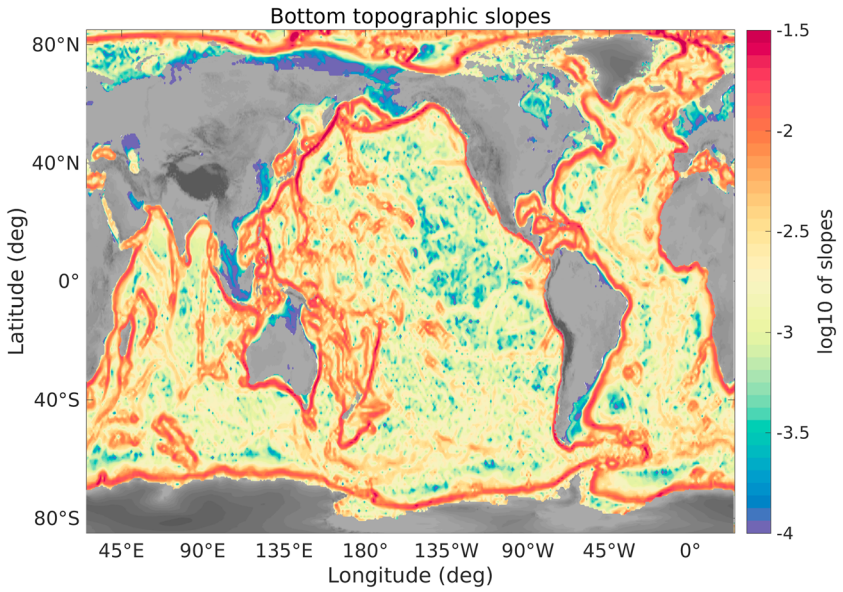

Figure 2. Bottom topographic slopes, with 100 km resolution, calculated from the etopo1 data set (https://www.ngdc.noaa.gov/mgg/global/).

velocity—and hence the cross-isobath velocity—is proportional to the vertical shear divided by the stratification, N^2. The latter is weak with exponential stratification, but the deep shear is even weaker (Figure 1b). In contrast, with constant stratification the deep shear actually *increases* with bottom slope (Figure 1a). With a slope of 10^{-4}, the bottom shear-to-N^2 ratio is 2 orders of magnitude smaller with exponential stratification than with constant stratification. The bottom velocities are similarly weaker.

The results for different size waves are similar. Shown in Figure 1c are the first eigenvalues with exponential stratification, plotted as a function of bottom slope. The corresponding values for the flat bottom BC1 and for the gravest surface mode are indicated for comparison. As noted, the inverse of the first eigenvalue is the mode's deformation radius, so the smaller eigenvalue for the surface mode implies that it has a larger deformation radius.

The eigenvalue is close to that of BC1 when the slope is weak and approaches the surface mode value when the slope is strong. But again, the transition between the two limits occurs for modest slopes. Shorter waves transition over weaker slopes, but in all cases the shift happens for slopes less than 10^{-4}, that is, a topographic grade of only 0.01%. The largest wave shown has a scale of 1,000 km, but larger waves yield essentially the same result as for that wave.

Thus, slopes greater than 10^{-4} should favor surface modes. But how large are the topographic gradients in the ocean? The answer depends on the lateral scale, but assuming a wave scale of 100 km yields the values contoured in Figure 2. The slopes vary with region, being largest near the continents and over the mid-ocean ridges. Nevertheless, they exceed 10^{-4} nearly everywhere. This suggests that the baroclinic modes should resemble surface modes in most of the ocean.

2.2. The Forced Ocean Response

Bathymetry affects the forced response similarly. We illustrate this with a simpler QG system, in which the stratification is represented by two layers of constant density (Pedlosky, 1987; Phillips, 1954; Vallis, 2006), with thicknesses of 1,000 m (upper) and 4,000 m (lower). The upper layer is forced by the wind, and the bottom slope lies entirely in the lower layer. This linear problem can also be solved analytically, as shown in section S2 of the supporting information.

We illustrate the response using wave number-frequency spectra of the upper layer stream function, obtained by solving the system neglecting variations in the y-direction (Figure 3a). The spectra reflect the upper layer response if the wind forcing has a white spectrum (as is often the case; Frankignoul and Hasselmann, 1977); different forcing spectra alter the amplitude of the response but not the general character. Without a bottom slope or friction, the system has two resonances, corresponding to BT and BC1

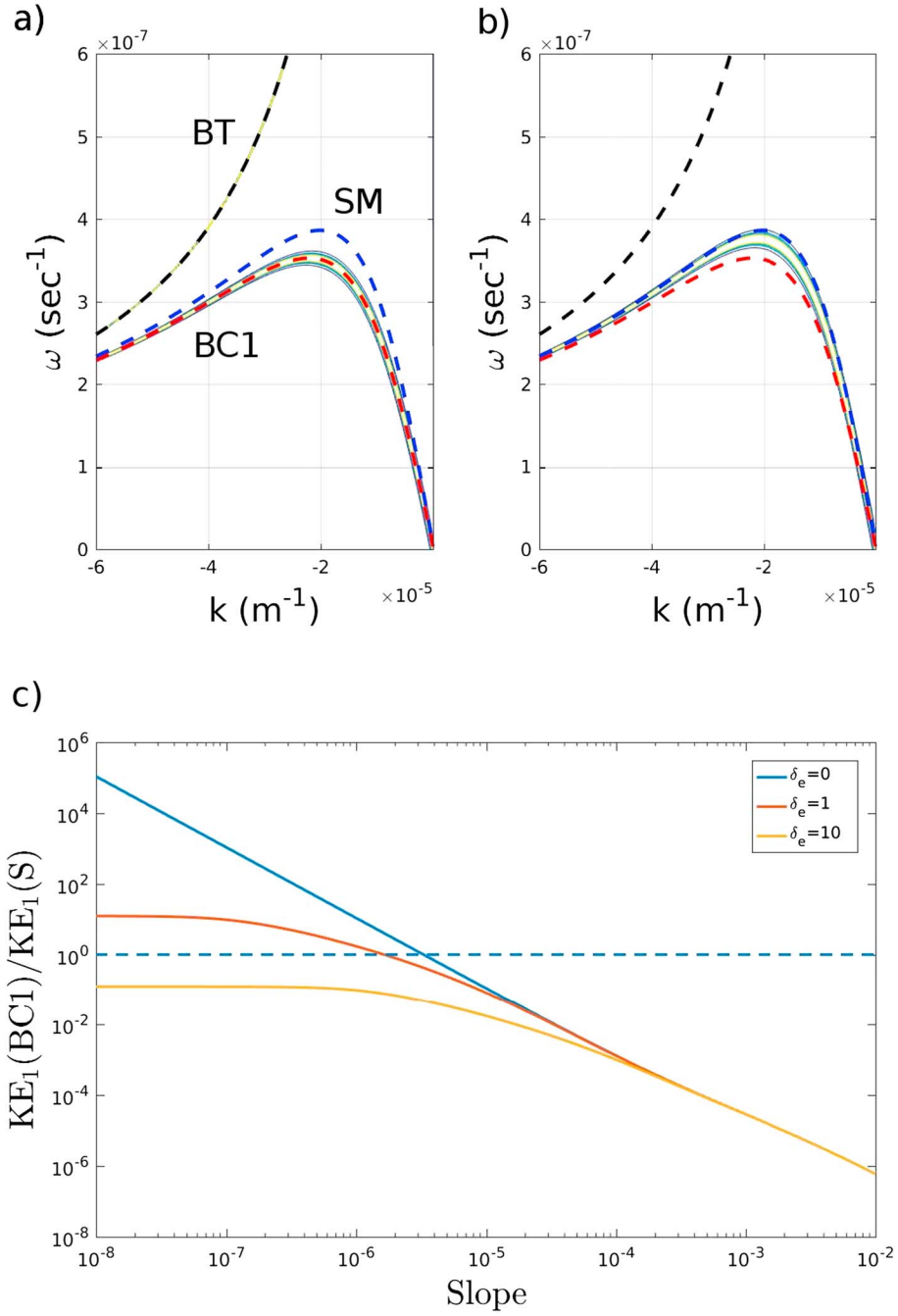

Figure 3. Wave number-frequency diagrams for the variance of the surface stream function from the linear two-layer model, with (a) a flat bottom and (b) a bottom slope of 10^{-3}. The contour intervals are from $[-5 : 5] \times 10^{34}$ m^4/s^2. Superimposed are the dispersion curves (given in supporting information S2) for the BT mode (dashed black), the flat bottom BC1 (dashed red), and the surface mode (dashed blue). (c) The ratio of the surface kinetic energy in the flat bottom BC1 to that in the surface mode, integrated over wave number. The blue curve corresponds to zero bottom friction, while the red and yellow curves have Ekman layer depths (δ_e) of 1 m and 10 m, respectively.

Rossby waves, and the upper layer response is accordingly greatest near the waves' dispersion curves (supporting information S2). With a bottom slope of 10^{-3}, the surface response is intensified instead near the dispersion curve for the surface mode Rossby wave, and the BT and BC1 modes are absent (Figure 3b). The response in the lower layer (not shown) is similar but weaker, but there is additional energy at higher frequencies and wave numbers, associated with topographic waves.

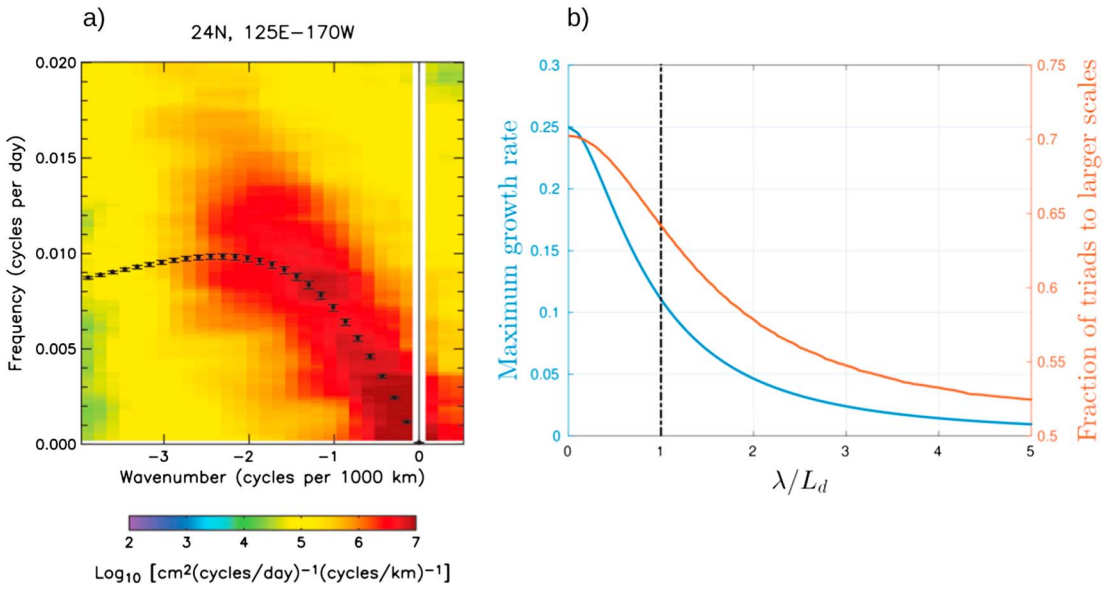

Figure 4. (a) The wave number-frequency spectrum from SSH measurements from 24°N in the Pacific, with the dispersion curve for a surface mode Rossby wave. Adapted from Figure 4 of Early et al. (2011) by J. Early. (b) The maximum growth rate (in blue) and the fraction of energy transferred to larger scales (in brown) for a surface mode Rossby wave, as a function of wavelength divided by the deformation scale, L_d.

Shown in Figure 3c is the ratio of the upper layer kinetic energy associated with BC1 to that in the surface mode. With no bottom friction (the blue curve), BC1 dominates for the smallest slopes. But as the slope increases, BC1 weakens and the surface mode intensifies, dominating for slopes exceeding 3×10^{-6}. With a slope of 10^{-3}, the surface mode kinetic energy is roughly a thousand times greater than that in BC1.

Bottom friction has relatively little effect over strong slopes, because the bottom velocities are already weak, but it does alter the response with weaker slopes. Friction in this model is represented by a (linear) Ekman layer, whose damping is proportional to its thickness. With a modest 1 m thick layer and a bottom slope of 10^{-8}, the energy in BC1 is reduced to only about 10 times that in the surface mode. With a more realistic Ekman depth of 10 m (Perlin et al., 2007; Weatherly & Martin, 1978), the surface mode dominates for *all* slopes. Note that an Ekman depth of 10 m corresponds to a friction coefficient of $R = 5 \times 10^{-4}$ m/s, a typical value used in ocean studies (Gill, 1982; Isachsen et al., 2003). Thus, bottom friction acts in a similar way, favoring the surface mode. Hence, the flat bottom baroclinic modes are applicable only over very weak slopes, without bottom friction.

2.3. Comparison With Surface Energy Spectra

Wave number-frequency spectra can be also calculated from sea surface height data (Wunsch & Stammer, 2010). A typical example is shown in Figure 4a, derived from data from the North Pacific (Early et al., 2011). The energy is clustered around a straight line for negative values of the wave number. This implies westward phase propagation at a constant speed, because the phase speed is the slope of the spectral curve. As demonstrated originally by Chelton and Schlax (1996), the phase speed inferred from such spectra is often faster than that of flat bottom BC1 Rossby waves. It is however similar to that of surface mode Rossby waves (Tailleux & McWilliams, 2001), and the spectrum in Figure 4a accordingly agrees with the surface mode dispersion curve at the smallest wave numbers. However, waves smaller than the deformation radius (the scale at which the dispersion curve is maximum) are conspicuously absent. Recall that the subdeformation scales are poorly resolved by altimetry, so this is also a contributing factor.

Using numerical experiments with a surface layer flow, Early et al. (2011) demonstrated that such wave number-frequency spectra are strongly affected by nonlinearity. In linear solutions with a random initial wave field, the resulting spectra resembled the surface wave dispersion curve, as shown in Figure 3. But in nonlinear simulations, the energy below the deformation radius shifted to larger scales, yielding spectra much like that in Figure 4a.

Such a shift is known as an inverse energy cascade, a phenomenon associated with turbulent two-dimensional flows and readily observed in numerical simulations (Fjørtoft, 1953; Fu & Flierl, 1980; Merilees & Warn, 1975; Rhines, 1977; Salmon, 1978). Surface Rossby waves exhibit a similar tendency, passing energy through

nonlinear interactions to larger waves, and this can be demonstrated analytically. Rossby waves interact in threes ("triads"), whose wave numbers and frequencies sum to zero. If the energy is initially in one wave, energy will flow to both a smaller and a larger wave, usually with a greater fraction going to the larger wave. If the initial wave is unstable, the secondary waves grow exponentially in time (Gill, 1974; Pedlosky, 1987). Such a calculation is given in section S3 of supporting information.

The maximum growth rate for a surface Rossby wave is plotted against the wave's initial scale in Figure (4b). The most rapid growth occurs for waves much smaller than the deformation radius, but the rate decreases markedly for larger waves. The fraction of kinetic energy transferred to larger scales also changes significantly with wave scale. With the smallest waves, over 70% of the energy is passed to the largest wave in the triad. But this fraction is nearer 50% when the initial wave is large. Thus, waves smaller than the deformation radius tend to pass energy rapidly to larger waves. This transfer then slows above the deformation radius, suggesting that larger waves should persist longer in the ocean interior.

In reality, small-scale oceanic eddies are less likely to be wave-like, but the tendencies are the same. Numerical simulations of surface flows over a resting lower layer indicate that the inverse cascade does slow at scales greater than the deformation radius (Cushman-Roisin & Tang, 1990; Early et al., 2011; Larichev & McWilliams, 1991). Thus, wave number-frequency spectra such as that in Figure 4a probably reflect an inverse cascade occurring below the deformation radius and stabler, larger features, propagating like surface mode Rossby waves. The latter are favored because bottom topography weakens the deep flow.

3. Discussion

The present results suggest that the preferred set of baroclinic modes in the ocean are the surface modes, with topographic waves accounting for velocity fluctuations at the bottom. This would explain the gravest EOFs of Wunsch (1997) and de La Lama et al. (2016), which resembled the gravest surface mode in many extratropical regions. As surface modes obtain with only modest bottom topography and friction, they should apply essentially everywhere in the ocean. Higher baroclinic modes are found with current meter data nearer the equator, but these modes also have nearly zero flow at the bottom (de La Lama et al., 2016).

The results have implications for the use of SSH data. Recently, it was shown that subsurface velocities could be reconstructed down to roughly 1,000 m depth knowing only the surface density and SSH, using a simplified version of the gravest surface mode (LaCasce & Wang, 2015). The density component was important only in the upper tens of meters; below that, the surface mode dominated. This suggests that subsurface velocities could be estimated from SSH alone using the gravest surface mode, and this only requires climatological density. Subsurface velocity reconstructions have numerous applications, from ocean prediction (e.g., of subsurface oil spills) to data assimilation in ocean models.

The prevalence of surface modes also affects how we interpret the dynamics of SSH anomalies. For one, it explains why they propagate faster than expected for flat bottom baroclinic Rossby waves (Chelton & Schlax, 1996; Tailleux & McWilliams, 2001). The phase speed of long Rossby waves is proportional to the square of the deformation radius, and since the surface mode has a larger deformation radius, it propagates faster. As noted, SSH anomalies at the 100 km scale are significantly nonlinear, having large advective speeds (Chelton et al., 2011). Such large vortices would be expected to be baroclinically unstable over a flat bottom, splitting into smaller vortices (Flierl, 1988; Helfrich & Send, 1988). However, bottom topography can stabilize large vortices (Hart, 1975; LaCasce, 1998). Thus, the presence of large, nonlinear eddies, propagating like Rossby waves, is probably an indication that bathymetry is hindering the spin-up of the deep layers.

The inverse energy cascade also occurs in the vertical, with energy shifting to graver modes. In turbulence simulations, energy inevitably arrives at the barotropic mode (Rhines, 1977). Barotropization is delayed with more realistic stratification but occurs eventually (Fu & Flierl, 1980; Smith & Vallis, 2001). The situation changes, however, with strong bathymetry and/or bottom friction (Arbic & Flierl, 2004; LaCasce, 2000), which favors surface intensification. As shown recently, the inclusion of (parameterized) topographic lee wave drag acts similarly, weakening the deep flow (Trossman et al., 2017). Thus, with realistic bathymetry and bottom drag, energy should accumulate in the gravest surface mode, rather than passing to the barotropic mode.

Perhaps most interesting is that the traditional barotropic mode probably does not exist. Barotropic Rossby waves, for example, are replaced by topographic waves. The latter have a vertical scale which depends on their horizontal wavelength, and waves much larger than deformation scale have significant surface flow.

Thus, large bathymetric features, like mid-ocean ridges or basins, could support topographic waves that are nearly barotropic. However, the sense of wave propagation for topographic waves is along isobaths rather than westward, and this affects how the ocean responds to surface forcing (Isachsen et al., 2003; Kamenkovich, 1962). Many fundamental theories of ocean circulation are based on barotropic, flat bottom idealizations (Anderson & Gill, 1975; Fofonoff, 1954; Munk, 1950; Stommel, 1948), and we must understand how the relevant concepts change if the barotropic mode is replaced by topographic waves.

A number of questions remain. The present arguments pertain to large-scale waves, and variability on smaller scales and at higher frequencies could differ. The current meter results of de La Lama et al. (2016) suggest that motions with periods as low as a day can also be described by the gravest surface mode, but the wider applicability of this result deserves further examination. To what extent linear baroclinic modes apply to nonlinear eddies must also be studied (despite that the modes are often used in describing such features).

There is also the issue of how energy is dissipated in such an ocean. With zero flow at the bottom, the surface mode is largely shielded from bottom friction. Energy must therefore pass to topographic waves to be dissipated. But how this occurs, whether at western boundaries (Zhai et al., 2010), over mid-ocean ridges (Barnier, 1988) or in regions with special topographic configurations (Hallberg, 1997; Straub, 1994), also deserves attention. The issue is important for assessing the dissipation of energy supplied by the winds (Wunsch & Ferrari, 2004).

In addition, the baroclinic modes examined here are applicable to a resting ocean. The derivations neglect mean flows, which can significantly alter the vertical structure and also produce deep flow via baroclinic instability (Berloff & Kamenkovich, 2013; Pedlosky, 1987). Instability is greatly affected by bottom topography (Benilov, 2001; Blumsack & Gierasch, 1972; Chen & Kamenkovich, 2013; Hart, 1975; Samelson & Pedlosky, 1990; Thompson & Sallée, 2012), which also can alter the vertical structure of the eddies generated. All such issues, relevant for nonflat oceans, need to be better understood.

Acknowledgments
The author is grateful to Jeffrey Early, Ada Gjermundsen, and Marta Sanchez de La Lama for help in preparing Figures (2) and (4a), and for comments on the original manuscript by Peter Rhines, Carl Wunsch, and two anonymous reviewers. The work was supported in part by grant 221780 (NORSEE) from Norges Forskningsrådet [10.13039/501100005416] (221780). The author declares that he has no competing financial interests. The scripts used in plotting the results shown in the paper are available on request from the author.

References

Anderson, D. L., & Gill, A. (1975). Spin-up of a stratified ocean, with applications to upwelling. *Deep Sea Research*, *22*, 583–596.
Anderson, D. L., & Killworth, P. E. (1977). Spin-up of a stratified ocean, with topography. *Deep Sea Research*, *24*, 709–732.
Arbic, B. K., & Flierl, G. R. (2004). Baroclinically unstable geostrophic turbulence in the limits of strong and weak bottom Ekman friction: Application to midocean eddies. *Journal of Physical Oceanography*, *34*, 2257–2273.
Barnier, B. (1988). A numerical study on the influence of the mid-Atlantic ridge on nonlinear first-mode baroclinic Rossby waves generated by seasonal winds. *Journal of Physical Oceanography*, *18*, 417–433.
Benilov, E. S. (2001). Baroclinic instability of two-layer flows over one-dimensional bottom topography. *Journal of Physical Oceanography*, *31*, 2019–2025.
Berloff, P., & Kamenkovich, I. (2013). On spectral analysis of mesoscale eddies. Part 1: Linear analysis. *Journal of Physical Oceanography*, *43*, 2505–2527.
Blumsack, S. L., & Gierasch, P. J. (1972). The effects of topography on baroclinic instability. *Journal of Atmospheric Sciences*, *29*, 1081–1089.
Charney, J., & Flierl, G. R. (1981). Oceanic analogues of large-scale atmospheric motions. In J. Charney & G. R. Flierl (Eds.), *Evolution of physical oceanography* (pp. 266–290). Cambridge, UK: MIT Press.
Chelton, D., & Schlax, M. (1996). Global observations of oceanic Rossby waves. *Science*, *272*, 234–238.
Chelton, D., Schlax, M., & Samelson, R. M. (2011). Global observations of nonlinear mesoscale eddies. *Progress in Oceanography*, *91*, 167–216.
Chen, C., & Kamenkovich, I. (2013). Effects of topography on baroclinic instability. *Journal of Physical Oceanography*, *43*, 790–804.
Cushman-Roisin, B., & Tang, B. (1990). Geostrophic turbulence and emergence of eddies beyond the radius of deformation. *Journal of Physical Oceanography*, *20*, 97–113.
de La Lama, M. S., LaCasce, J. H., & Fuhr, H. (2016). The vertical structure of ocean eddies. *Dynamics and Statistics of the Climate System*, *1*, dzw001.
Early, J., Samelson, R., & Chelton, D. (2011). The evolution and propagation of quasigeostrophic ocean eddies. *Journal of Physical Oceanography*, *41*, 1535–1555.
Fjørtoft, R. (1953). On the changes in the spectral distribution of kinetic energy for two dimensional, non-divergent flow. *Tellus A*, *5*, 225–230.
Flierl, G. R. (1988). On the instability of geostrophic vortices. *Journal of Fluid Mechanics*, *197*, 349–388.
Fofonoff, N. P. (1954). Steady flow in a frictionless homogeneous ocean. *Journal of Marine Research*, *13*, 254–262.
Frankignoul, C., & Hasselmann, K. (1977). Stochastic climate models, part 2, application to sea surface temperature anomalies and thermocline variability. *Tellus A*, *29*, 289–305.
Fu, L. L., & Flierl, G. R. (1980). Nonlinear energy and enstrophy transfers in a realistically stratified ocean. *Dynamics of Atmospheres and Oceans*, *4*, 219–246.
Fu, L. L., Keffer, T., Niiler, P. P., & Wunsch, C. (1982). Observations of mesoscale variability in the western North Atlantic; a comparative study. *Journal of Marine Research*, *40*, 809–848.
Garrett, C. (1978). Topographic Rossby waves off east Australia: Identification and role in shelf circulation. *Journal of Physical Oceanography*, *9*, 244–253.
Garrett, C., & Munk, W. (1972). Space-time scales of internal waves. *Geophysical Fluid Dynamics*, *2*, 225–264.
Gill, A. E. (1974). The stability of planetary waves on an infinite beta plane. *Geophysical and Astrophysical Fluid Dynamics*, *6*, 29–47.
Gill, A. E. (1982). *Atmosphere-ocean dynamics* (662 pp.). London: Academic Press.

Hallberg, R. (1997). Localized coupling between surface and bottom-intensified flow over topography. *Journal of Physical Oceanography*, *27*, 977–998.
Hart, J. E. (1975). Baroclinic instability over a slope. Part 1: Linear theory. *Journal of Physical Oceanography*, *5*, 625–633.
Helfrich, K. R., & Send, U. (1988). Finite-amplitude evolution of two-layer geostrophic vortices. *Journal of Fluid Mechanics*, *197*, 331–348.
Isachsen, P., LaCasce, J., Mauritzen, C., & Häkkinen, S. (2003). Wind-driven variability of the large-scale recirculating flow in the Nordic Seas and Arctic Ocean. *Journal of Physical Oceanography*, *33*, 2534–2550.
Kamenkovich, V. (1962). On the theory of the Antarctic circumpolar current. *Trudy Instituta okeanologii*, *56*, 245–306.
Kundu, P., Allen, J., & Smith, R. (1975). Modal decomposition of the velocity field near the Oregon coast. *Journal of Physical Oceanography*, *5*, 683–704.
LaCasce, J. H. (1998). A geostrophic vortex on a slope. *Journal of Physical Oceanography*, *28*, 2362–2381.
LaCasce, J. H. (2000). Geostrophic turbulence over a slope. *Journal of Physical Oceanography*, *30*, 1305–1324.
LaCasce, J. H. (2012). Surface quasigeostrophic solutions and baroclinic modes with exponential stratification. *Journal of Physical Oceanography*, *42*, 569–580.
LaCasce, J. H., & Wang, J. (2015). Estimating subsurface velocities from surface fields with idealized stratification. *Journal of Physical Oceanography*, *45*, 2424–2435.
Larichev, V. D., & McWilliams, J. C. (1991). Weakly decaying turbulence in an equivalent barotropic fluid. *Physics of Fluids A*, *3*, 938–950.
Merilees, P., & Warn, H. (1975). On energy and enstrophy exchanges in two-dimensional non-divergent flow. *Journal of Fluid Mechanics*, *69*, 625–630.
Munk, W. H. (1950). On the wind-driven ocean circulation. *Meteorology*, *7*, 80–93.
Munk, W. H. (1966). Abyssal recipes. *Deep Sea Research*, *13*, 707–730.
Pedlosky, J. (1987). *Geophysical fluid dynamics* (2nd ed., 728 pp.). New York: Springer.
Perlin, A., Moum, J. N., Klymak, J. M., Levine, M. D., Boyd, T., & Kosro, P. M. (2007). Organization of stratification, turbulence, and veering in bottom ekman layers. *Journal of Geophysical Research*, *112*, C05S9. https://doi.org/10.1029/2004JC002
Phillips, N. A. (1954). Energy transformations and meridional circulations associated with simple baroclinic waves in a two-level, quasi-geostrophic model. *Tellus A*, *6*, 273–286.
Pickart, R. (1995). Gulf stream-generated topographic Rossby waves. *Journal of Physical Oceanography*, *25*, 574–586.
Rhines, P. (1970). Edge-, bottom-, and Rossby waves in a rotating stratified fluid. *Geophysical and Astrophysical Fluid Dynamics*, *1*, 273–302.
Rhines, P. B. (1977). The dynamics of unsteady currents. *The Sea*, *6*, 189–318.
Salmon, R. (1978). Two-layer quasi-geostrophic turbulence in a simple special case. *Geophysical and Astrophysical Fluid Dynamics*, *10*, 25–52.
Samelson, R. M. (1992). Surface-intensified Rossby waves over rough topography. *Journal of Marine Research*, *50*, 367–384.
Samelson, R. M., & Pedlosky, J. (1990). Local baroclinic instability of flow over variable topography. *Journal of Fluid Mechanics*, *221*, 411–436.
Smith, K. S., & Vallis, G. K. (2001). The scales and equilibration of midocean eddies: Freely evolving flow. *Journal of Physical Oceanography*, *31*, 554–571.
Stammer, D. (1997). Global characteristics of ocean variability estimated from regional Topex/Poseidon altimeter measurements. *Journal of Physical Oceanography*, *27*, 1743–1769.
Stommel, H. (1948). The westward intensification of wind driven ocean currents. *Eos*, *29*, 202–206.
Straub, D. N. (1994). Dispersion of Rossby waves in the presence of zonally varying topography. *Geophysical and Astrophysical Fluid Dynamics*, *75*, 107–130.
Tailleux, R., & McWilliams, J. C. (2001). The effect of bottom pressure decoupling on the speed of extratropical, baroclinic Rossby waves. *Journal of Physical Oceanography*, *31*, 1461–1476.
Thompson, A., & Sallée, J. (2012). Jets and topography: Jet transitions and the impact on transport in the Antarctic circumpolar current. *Journal of Physical Oceanography*, *42*, 956–972.
Trossman, D., Arbic, B., Straub, D., Richman, J., Chassignet, E., Wallcraft, A., & Xu, X. (2017). The role of rough topography in mediating impacts of bottom drag in eddying ocean circulation models. *Journal of Physical Oceanography*, *47*, 1941–1959.
Vallis, G. K. (2006). *Atmospheric and oceanic fluid dynamics: Fundamental and large-scale circulation* (1st ed., p. 745). Cambridge, UK: Cambridge University Press.
Veronis, G. (1981). Dynamics of large-scale ocean circulation. In G. Veronis (Ed.), *Evolution of physical oceanography* (pp. 140–183). Cambridge, UK: MIT Press.
Weatherly, G. L., & Martin, P. J. (1978). On the structure and dynamics of the oceanic bottom boundary layer. *Journal of Physical Oceanography*, *8*, 557–570.
Wunsch, C. (1997). The vertical partition of oceanic horizontal kinetic energy. *Journal of Physical Oceanography*, *27*, 1770–1794.
Wunsch, C. (2015). *Modern observational physical oceanography: Understanding the global ocean* (493 pp.). Princeton, NJ: Princeton University Press.
Wunsch, C., & Ferrari, R. (2004). Vertical mixing, energy, and the general circulation of the oceans. *Annual Reviews of Fluid Mechanics*, *36*, 281–314.
Wunsch, C., & Stammer, D. (2010). The global frequency-wavenumber spectrum of oceanic variability estimated from topex/poseidon altimetric measurements. *Journal of Geophysical Research*, *100*, 24,895–24,910. https://doi.org/10.1029/95JC01783
Zang, X., & Wunsch, C. (2001). Spectral description of low-frequency oceanic variability. *Journal of Physical Oceanography*, *31*, 3073–3095.
Zhai, X., Johnson, H. L., & Marshall, D. P. (2010). Significant sink of ocean-eddy energy near western boundaries. *Nature Geoscience*, *3*, 608–612.